Validation of a Flame Tranfer Function Reconstruction Method for Complex Turbulent Configurations

A. Giauque*
CTR Stanford University, Stanford, CA., 94305, USA

T. Poinsot†
Institut de Mecanique des Fluides de Toulouse, Toulouse, 31400, France

W. Polifke‡
TU Muenchen Lehrstuhl fuer Thermodynamik , Garching, D-85747, Germany

F. Nicoud§
Universite Montpellier II I3M, Montpellier, 34095, France

September 21, 2007

1 Abstract

Flame Transfer Functions (FTFs) are now an important "brick" of acoustic analysis used for the design of complex turbulent combustors. Two different methods for the determination of FTFs in LES are compared. **HF-FFT** method, based on harmonic flame forcing and FFT post-processing is known to give results of global combustion delays that compare well with the experiments [1].
A new **WN-WH** method based on filtered-white noise forcing and post-processing using the Wiener-Hopf relation is successfully compared to **HF-FFT**. Though this method should be handled with care, its main advantage is that it gives access to the frequency spectrum of the local FTF with lower computational cost.
This method provides the local FTF which gives valuable information about the amplitudes, delays and maximum locations of the local flame response. This method should reveal useful for configurations where the response of the flame is not compact compared to the characteristic wavelength of the excitation, as

*Postdoctoral Fellow, CTR Stanford University, Stanford ,CA., USA
†Research Director, IMFT, Toulouse, France.
‡Professor Ph.D.(CCNY), TU Muenchen, Garching, Germany
§Professor, Universite Montpellier II I3M, Montpellier, France

for distributed reacting cases.
This study is closely linked with stability analysis of combustors. Obviously, FTFs do have an influence on the frequency and amplification rates of modes in the numerical methods used for combustor stability.

2 Introduction

Modern pollutant emission regulation policies have lead combustion engines industry to consider using more lean premix combustion instead of diffusion which creates greater concentrations of pollutant in the burnt gases. Because in this regime the stable position of the flame is directly linked to the surrounding flow, Flame-acoustic coupling is somewhat stronger and may lead to thermo-acoustic instabilities. Flame acoustic coupling is a phenomenon which is found in multiple combustors[2, 3, 4, 5]. To prevent the appearance of thermo-acoustic instabilities at an early stage of the design, one need information on the dynamic behavior of the combustion process. However, predicting flame / acoustics coupling is still a challenge [6, 7, 8] and no satisfying analytical model describing this interaction exist for real reactive geometries. In this case, only sophisticated numerical methods can be used to characterise burner responses while at the design stage. LES (Large Eddy Simulations) is now the most precise numerical tool for turbulent flames as shown by numerous recent examples [4, 9, 10]. The dynamic behavior of the flame can be represented thanks to the Flame Transfer Function (FTF) first introduced by Crocco [11]. This information is given in form of a 1D function, relating flow variables as a function of frequency or pulsation. This function is defined as:

$$\frac{\hat{Q}'}{\bar{Q}} = F(\omega)\frac{\hat{u}'}{\bar{u}} \tag{1}$$

which relates the Fourier transformed velocity fluctuation upstream of the flame (usually at the inlet of the combustion chamber) to the volume integral of the heat release fluctuation (Q) caused by the flame as a function of pulsation ω.

In this paper, two methods used to obtain the FTF using LES are compared:

- Harmonic forcing; FFT postprocessed method (HF-FFT method)
  This method consists in introducing a downstream acoustic wave at a fixed pulsation (ω) into the system. The response of the flame at this same pulsation is obtained through the Fourier transform of the heat release fluctuation integrated over the whole domain of simulation.

- White noise forcing; Wiener-Hopf postprocessed method (WN-WH method)
  This method using white-noise forcing and the Wiener-Hopf relation inversion was introduced in FTF measurements by Schuermans et al. [12] and used by many authors [13, 14, 15, 16]. To use this method, the inlet has to be forced with a filtered white-noise including all frequencies below

a given cut-off frequency. The main advantage of this method is to give the FTF frequency dependance with only one reactive LES.

The first objective of this paper is to validate WN-WH method against HF-FFT method in a realistic turbulent reactive configuration by comparing the amplitude and the phase of the FTF measured using both methods.
Results obtained with both methods will finally be compared using the Local FTF. The local dimensional 3D response of the flame is defined by

$$\hat{\dot{\omega}}'_T(x,y,z) = F_{3D}(x,y,z,\omega)\hat{u}' \tag{2}$$

where F_{3D} compares the local fluctuation of heat release to the fluctuation of reference velocity, $\hat{\dot{\omega}}'_T$ is the Fourier transform of the local heat release fluctuation and $\hat{u}'$ is the Fourier transform of the forced inlet velocity.
Analysing the local 3D FTF gives insight into the repartition of the FTF along the flame front. It is shown that even if global FTF are similar using both methods, differences may be found in the local repartition of the FTF.

The LES tools and the numerical methodology used to introduce acoustic waves through boundaries are first presented.Then the two methods used for FTF measurements (HF-FFT and WN-WH methods) are described.A brief analysis of the behavior of a forced 1D flame is provided for its main features also appear in 3D turbulent cases.A comparison of LES results obtained with the two methods is performed in terms of amplitude and phase of the FTF between inlet velocity and global heat release.Finally, a local analysis of the flame response is described to compare LES results obtained with HF-FFT and WN-WH methods.

3 Numerical LES tool

3.1 LES as the proper tool for FTF

Considering the measurement of turbulent FTF, the advantage of LES is clear [4, 17, 18, 19, 20, 21, 22]. Turbulent FTF are mainly needed for acoustic study purposes in complex geometries. Typical acoustic frequencies are of the order of 500 Hz in gas turbines corresponding to a period of 2 ms which correspond to time scales that are now affordable for LES even in complex geometries thanks to the use of unstructured meshes.
To determine FTF, one needs either the instantaneous volume integral of the heat release fluctuation (to determine the global response of the flame) or the instantaneous field of heat release fluctuations (to determine the local response of the flame). In this paper, LES (AVBP code from CERFACS (www.cerfacs.fr/cfd)) is chosen to get these fields.
AVBP is used to solve the full compressible Navier Stockes equations on unstructured grids with third-order spatial and temporal accuracy [19]. Subgrid stresses are described by the WALE model [23]. The subgrid flame / turbulence

interaction is modelled by the Thickened Flame (TF) model [17, 24]. The validity of the TF model used here has been checked in many recent papers [4, 25] and will not be discussed here.
For the present application, methane / air combustion is modelled using six species (CH_4,O_2, CO_2, CO, H_2O and N_2) and two reactions [26]. These reactions are :

$$CH_4 + 3/2O_2 => CO + 2H_2O \tag{3}$$

$$CO + 1/2O_2 <=> CO_2 \tag{4}$$

The forward rate of the first irreversible reaction is:

$$q_1 = AY_{CH_4}^{0.9}\, Y_{O_2}^{1.1}\, exp(-T_a^1/T)$$

and the rate of the second reaction is:

$$q_2 = B[Y_{CO}\, Y_{O_2}^{0.5} - (1/K_y)\, Y_{CO_2}]\, exp(-T_a^2/T)$$

where $A = 6.1.10^8\ mol.m^{-3}.s^{-1}$, $B = 6.1.10^5\ mol.m^{-3}.s^{-1}$, $T_a^1 = 17613$ K, $T_a^2 = 6038$ K and $K_y(T)$ is the equilibrium constant of reaction (2).

3.2 Introducing acoustic waves through the burner inlet

To determine the transfer function of a burner, the usual procedure is to introduce an acoustic wave into the burner (usually through the inlet) and measure the perturbation of heat release. The phase between the incoming unsteady flow rate and the unsteady heat release is an essential ingredient of acoustic approaches for combustor stability [27, 28, 29, 30, 31, 13]. However, the exact numerical procedure to introduce acoustic waves in a computation is a difficult topic and may lead to numerical artefacts [32, 33]. In subsonic compressible LES, each boundary must be specified in terms of mean conditions (velocity or pressure for example) but also in terms of acoustic impedance. Many methods for such problems are based on characteristic methods [34, 31] but must be used with care: the well - known 'non reflecting' conditions actually impose an impedance (which is often unknown) and can have a strong influence on the results [4]. For a simple laminar flame, Kaufmann et al [35] show that a proper method to excite a combustion chamber is to pulsate the incoming acoustic wave and not the incoming local velocity. This procedure is used here and avoids false numerical resonances when the chamber is forced. The acoustic wave is therefore introduced into the combustion chamber through the inlet.
An issue when forcing such a configuration comes from the amplitude of the waves reflected at the chamber outlet which must remain low in order to minimise self-excited oscillations. This is done using the NSCBC boundary method [36, 33, 31] which allows the control of the acoustic impedances on the boundaries.

4 Flame Tranfer Function measurement methods

4.1 Harmonic forcing; FFT postprocessed method (HF-FFT method).

This method consists in introducing a downstream acoustic wave at a fixed pulsation (ω) as described previously. It assumes that the response to a harmonic perturbation of the flow is a harmonic fluctuation of heat release. The global FTF is obtained through equation 1 and the local flame transfer function from equation 2. The method to retrieve the FTF can be described in the local case as follows.

- Harmonically forced Large Eddy Simulations of the configuration are done for a discrete set of excitation frequencies.
- 3D fields of heat release fluctuation are extracted as well as the reference (usually the inlet) velocity fluctuation.
- 3D fields of $F_{3D}(\omega)$ are obtained using FFTs of $\dot{\omega}'_T(t)$ and $u'(t)$ and by constructing $F_{3D}(\omega)$ through equation 2. $F_{3D}(\omega)$ is a local information about the location and the phase of the flame response.

This method requires FFTs of $\dot{\omega}'_T$ at all points of the combustor during its forced operation. In the present work, this is obtained by using typically 100 snapshots with 10 snapshots per period which gives a frequency resolution of 1/10th of the forcing frequency. This method is expensive because it must be repeated for a representative set of discrete frequencies (typically 5 to 10), leading to many forced LES.

4.2 White noise forcing; Wiener-Hopf postprocessed method (WN-WH method).

To use this method, the inlet has to be forced with a filtered white-noise including all frequencies below a given cut-off frequency. This method takes advantage of the Wiener-Hopf equation linking the autocorrelation matrix Γ of the inlet signal (inlet velocity) and the cross-correlation vector c :

$$\Gamma h = c \tag{5}$$

where h is the impulse response filter (i.e the filter corresponding to the unit response of the system). However here, h corresponds to the white-noise response filter.
The method to retrieve the FTF(F_{3D}) can be described as follows:

- A LES forced with filtered white noise is performed.
- The response signal (local heat release) and the reference signal (inlet velocity) are stored.

- Knowing the white noise inlet velocity signal (s), the autocorrelation matrix Γ can be determined:

$$\Gamma_{i,j} = \frac{1}{M}\sum_{l=L}^{N} s_{l-i}s_{l-j} \ for \ i,j \ = \ 0,...,L. \ {}_{(M=N-L+1)} \tag{6}$$

- Using the inlet (velocity)(s) and the response (heat release)(r) signals, the cross-correlation vector can be obtained :

$$c_i = \frac{1}{M}\sum_{l=L}^{N} s_{l-i}r_l \ for \ i \ = \ 0,...,L. \tag{7}$$

  so that the equation 5 can be inverted to obtain h.

- Using relation 8, the FTF is obtained from the filter h.

$$\sum_{k=0}^{L} h_k e^{-i\omega\Delta tk} = 1 + F_{3D}(\omega) \tag{8}$$

The parameter L is the length of the filter and is critical to the validity of this analysis. ΔtL represents the time memory of the filter. It means that the biggest time delay τ_{max} available is determined by the value of L ($\tau_{max} = \Delta tL$). Attention has also to be paid not to choose L too big to avoid numerical problems during the inversion of the Γ matrix since its size varies like L^2.
The greatest advantage of this method is that it gives full three dimensional fields of the amplitude and the phase response of the flame. It is also able to give the response parameters at all frequencies below the given cut-off frequency with only one forced LES.

5 FTF of a laminar planar 1D premixed flame

A 1D flame is forced with an incoming acoustic wave at $200Hz$ with an amplitude of 0.5 $m.s^{-1}$. The reference point for the velocity is the domain inlet. The distance between this point and the mean flame front is 1mm. The mean inlet velocity is equal to the laminar flame speed so that the flame is stable when there is no forcing. The dimensions of the structured mesh are 2.10^{-2}m $\times$ 2.10^{-9}m. Figure 1 sums up the numerical experiment and shows the location of three sample points A, B and C. The flame width is 0.5mm and the pulsated flame "extension" (the zone over which the flame moves during forcing) is 1mm. Signals of heat release are collected along a line crossing the flame. Figure 2 gives the heat release signals at points A, B and C (normalized by the maximum value) as well as the reference inlet velocity. It is interesting to note that signals of heat release are not harmonic because the pulsated flame extension is greater than the flame width. This particular feature is encountered in 3D turbulent configurations since the pulsated velocity amplitude at the flame front is even higher than the present value.

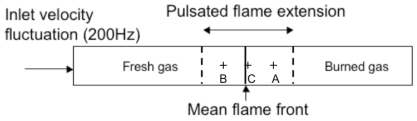

Figure 1: numeric experimental setup.

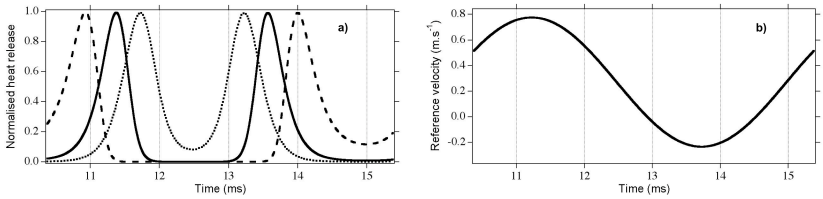

Figure 2: a) Signals of heat release at points - - - A, — — B and —— C. b) Reference velocity signal

5.1 Amplitude

Figure 2 shows that the maximum instantaneous heat release is the same for all three points. But the amplitude of the response, normalized by the maximum local response differs between A and B and C, as presented on table 1. The response at point C which is in the mean flame is almost negligible because the frequency of the heat release fluctuating signal at that point is not 200Hz. Actually, the flame passes exactly twice at that location during a period, so that the response at the mean flame position is mainly at 400Hz. The 200 Hz component increases as one approaches from the maximum extension position of the forced flame front as shown on figure 3.

	Point A	Point B	Point C
Amplitude	0.462	0.555	0.068

Table 1: Normalized amplitude of the response at points A, B and C (HF-FFT)

5.2 Time delay

At points A and B, the flame has almost the same amplitude of response, but very different time delays. Point B is closer to the forced inlet. One therefore expects that the time delay at that point will be smaller. It is not the case and table 2 sums up the time delays for points A and B . Point A has the lowest time delay, and since this point is farer than B from the inlet, it is interesting to explain this result.
In the present case, the pulsated flame zone is compact when compared to the

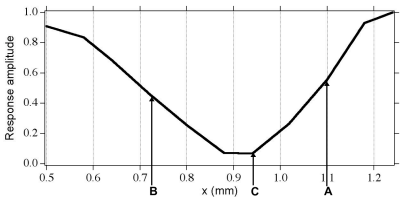

Figure 3: Normalized amplitude of the response along the axial line.

acoustic wavelength which is 1.7m long. Therefore, the velocity fluctuation at point C (which is at the mean flame position) is almost in phase with the inlet velocity. When the velocity at the inlet increases, it pushes the flame from C to A. The flame first reaches that point before the inlet velocity decreases and comes back to C. After more than half a period, the flame reaches B. In this case the flame mean position therefore separates two differents zones of time delays with a discontinuity of half the time period. Figure 4 represents the values of time delays along the axial line crossing the mean flame position. This type of behavior is also observed in 3D cases where time delays exhibit abrupt changes at the mean flame position.

	Point A	Point B
Time delay (ms)	1.228	3.761

Table 2: Time delays at points A, B

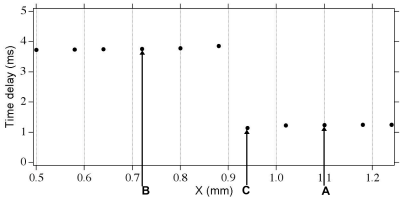

Figure 4: Time delay (ms) of the flame response along the axial line.

6 Numerical configuration used for FTF measurements

The burner is a modified version of a single Siemens hybrid burner used here at atmospheric pressure (maximum power = 400 kW). This burner is mounted on a sector of an annular chamber (see Figure 5). The simulation includes a 15

degrees sector of the whole combustion chamber. Side faces are enclosed with slip adiabatic rigid walls. The mesh contains 339417 nodes and 1859248 tetrahedral elements. Fully premixed methane / air is injected through two coaxial swirlers (diagonal and axial) at an equivalence ratio of 0.8 for the axial and 0.5 for the diagonal swirler. The flow rates injected in the combustion chamber are respectively $0.018kg.s^{-1}$ for the axial and $0.162kg.s^{-1}$ for the diagonal swirler.

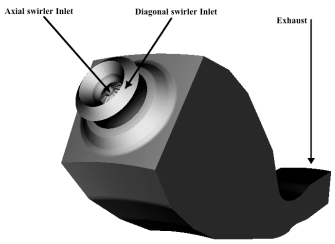

Figure 5: Burner mounted on an annular combustion chamber.

Validation concerning mean and RMS results will not be presented here. This same mesh has been used to explore the influence of piloting on combustion stability [37]. By adding two side burners to this configuration, it is also used by Staffelbach et al. [38] to evaluate the influence of the extension of the mesh on the resulting unstable modes of the configuration.

6.1 General computational remarks.

Two main methods using LES to get the FTF are compared. The first method (HF-FFT method) requires the injection of a harmonic signal at the main inlet of the configuration. The frequency of forcing is changed to get the dependance of the FTF to frequency. The configuration is forced at six frequencies between 90 and 540 Hz.
With an explicit resolution of the Navier-Stokes equations and a time step of the order of $4.0e^{-7}s$, 25000 iterations are needed to compute one period if the configuration is forced with a 100 Hz acoustic wave. Since the HF-FFT method uses the Fourier transform of signals, the spectral resolution is equal to the inverse of the total computed time. Therefore, to get a resolution of 20Hz, 0.05s have to be computed, which corresponds to 125000 explicit iterations. On 64 processors on a CRAY XD1, it represents 50h of computation. Therefore, no calculations for lower frequencies than 90Hz have been made to save computational time.
Since WN-WH method is based on the correlation of signals and not on their Fourier transform, theoretically only one period has to be resolved to state for

the time delay. Yet, to enable a simpler comparison between the two methods, they are applied on the same fields of heat release and velocity fluctuations corresponding to a minimum of five periods for all concerned frequencies.

Table 3 summarizes the physical simulated times and CPU costs for the turbulent case and for the three methods. All computations have been done on a CRAY XD1 (64 processors).

Forcing method	physical time	CPU cost
HF-FFT	22-55ms	192h
WN-WH	55ms	54h

Table 3: Comparison of the computational costs and simulated times for the two forcing methods.

No less than five periods have been computed for the harmonically forced cases. Since different computations have to be done for each frequency when using HF-FFT method, the cost of this method is four times bigger.

6.2 Reference signals

For both methods, investigations of global and local FTF are done. Depending on global or local FTF analysis, different response signals have to be compared to the reference signal.

6.2.1 Comparison of global FTF.

In this case, the reference inlet velocity signal is the harmonic or white-noise fluctuating velocity, and the response signal is the integrated heat release fluctuation over the whole volume. Figure 6 presents these signals for the turbulent configuration and for the white noise forced case. Inlet velocity and heat release signals are normalized by their mean values. There is a clear correlation between these two signals. One can observe that a maximum of inlet velocity induces a maximum of heat release after approximately 2-3 ms .

6.2.2 Comparison of local FTF.

In this case, 3D fields of heat release fluctuation are used. The transfer function of each grid point is calculated using HF-FFT and WN-WH methods. Figure 7 shows a 2D longitudinal cut colored with the instantaneous local heat release. The LES are done using the optimal local flame thickening model [39] with 7 points in the flame front. It leads to a thickening factor ranging from approximately 5 to 50 depending on the local refining of the mesh. A point shows the location of the reference inlet point.

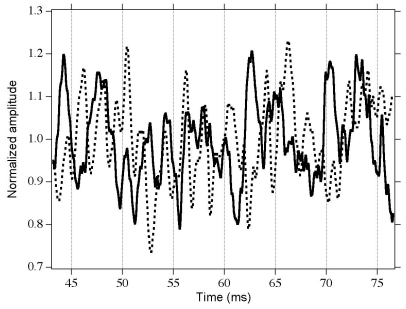

Figure 6: Normalized signals of reference for the white-noise forced case: —— inlet velocity - - - heat release

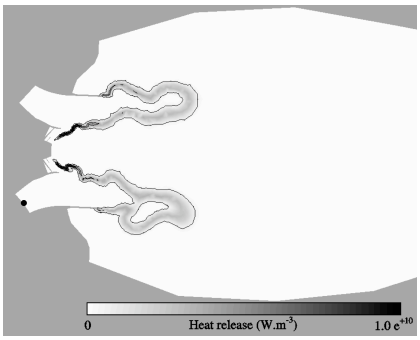

Figure 7: 2D longitudinal cut colored by instantaneous heat release. Black point marks the reference inlet point.

7 Results

7.1 Comparison of global FTF (F)

7.1.1 Amplitude

Figure 8 presents the amplitudes of the FTF obtained with HF-FFT and WN-WH methods from signals of Fig.(6). It appears that HF-FFT and WN-WH methods give similar results for the amplitude of the turbulent FTF, with a minimum taken from the Wiener-Hopf curve at approximately 300Hz. Figure 8 also shows that the result obtained with WN-WH method is sensitive to the size of the filter used to compute auto-correlation matrix and cross-correlation vectors. Depending on the value chosen for the filter length L, the response experiences a variation of approximately 10 percent. When approaching the cut-off frequency (600 Hz) of the low pass filter used to obtain the white noise signal, the discrepancy between results for different L values increases. The

amplitude of the FTF is lower than one for the frequencies of interest. It means that the relative fluctuation of heat release is lower than the relative fluctuation of the inlet velocity for all frequencies. Figure 8 shows that a maximum of the FTF amplitude is reached around 500Hz. If the inlet velocity is forced at 10% of its mean value at 500Hz, the heat release will fluctuate with an amplitude of 8% of its mean value.
Using Eqs.(9), the normalized amplitude of $|F|$ at 100Hz can be estimated. It is equal to 1.77. This value can be compared to the asymptotic value given by Eq.(12). With a mean temperature of 1835K in burnt gases and a temperature of 685K at the inlet, the asymptotic value of the interaction index for low frequencies is equal to 1.68. The value for $|F|$ at 100Hz therefore compares well with this theoretical amplitude.

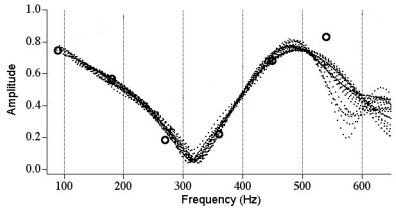

Figure 8: Amplitude of FTF : ∘ HF-FFT method. **....** WN-WH method for various values of the filter size L.

7.1.2 Phase

Figure 9 compares the global time delays obtained with HF-FFT and WN-WH methods. HF-FFT and WN-WH time delays almost match for all frequencies. Results show a discontinuity around 300Hz. This artefact is only due to the phase crossing the 2π limit and going back to zero. Without reference time for the delay, values above 300 Hz are either τ or $T + \tau$ without changing the phase between the heat release fluctuation and the reference velocity fluctuation. Though, fluctuations (depending on L) of the results of Wiener-Hopf relation's inversion are important near 300 Hz and 600 Hz. The last frequency corresponds to the cut-off frequency and has already been pointed out concerning the amplitude analysis. The source of fluctuations around 300 Hz is not clear but corresponds to the fact that the phase crosses the 2π limit for slightly different frequencies depending on the value of the L parameter.

7.2 Local comparison of FTF (F_{3D})

It has been shown in the previous section that the global response of the system is almost identical when forced with a harmonic signal or with a filtered white noise. It is therefore interesting to focus on the local response of the flame. The

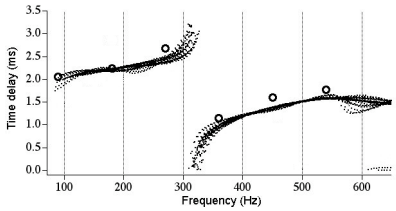

Figure 9: Time delay of FTF : ∘ HF-FFT method. **....** WN-WH method (for various values of the filter size L).

analysis is done by comparing results obtained with the two methods HF-FFT and WN-WH at 90 Hz. the WN-WH method gives the FTF for all the frequency range included in the spectrum of the imposed filtered white noise. Results at 90 Hz are therefore extracted from the total resolved spectrum for the WN-WH method. The frequency of 90Hz was chosen because it is the value observed experimentally in the full combustor (it is an azimutal mode). Longitudinal cuts colored by the local amplitude and time delay are used to support this analysis. Finally the weighted probability density function of time delays for both cases is commented.

7.2.1 Amplitude

Figures 10 and 11 show 2D longitudinal plane cuts colored by the amplitude of the FTF at 90Hz, respectively obtained using the HF-FFT and WN-WH methods. Note that the mean flame position is slightly different whether the flame is forced using HF-FFT method or WN-WH method. This is due to the fact that the simulation time is not long enough to ensure a perfect convergence of the mean heat release field.
Figure 10 shows that the response amplitude to the 90Hz acoustic excitation is almost axi-symmetric although the geometry of the combustion chamber is not. It means that the shape of the forced flame is mostly imposed by the injector which is axi-symmetric. The 2D plane cut colored by the response amplitude is separated in two zones which react differently to the excitation.

- In Zone 1, the response amplitude is intense. It corresponds to high values of local heat release fluctuations. This is due to the equivalence ratio of the axial swirler ($\phi = 0.8$) which is higher than the equivalence ratio of the diagonal swirler ($\phi = 0.5$). The mean heat release in this zone is therefore higher and leads to more heat release fluctuations for a given incoming velocity fluctuation.

- In Zone 2 the level of mean heat release is almost constant along the flame front but the side anchored at the burner mouth and the side stabilized by the precessing vortex core [1, 40] show differences in their response amplitude to the fluctuation. The part of the flame front attached to the

outer part of the burner reacts more weakly to the perturbation showing that this part of the flame is well anchored and less prone to instability.

The separation of the response of the white noise forced flame in two zones is not so clear on figure 11 : some parts of the zone 2 show a response which has the same amplitude as in zone 1. The response amplitude is not perfectly axi-symetric. This can be due to the effects of the geometry in the case of the white-noise forced flame. Also note that as for the harmonically forced case, the outer flame front reacts less intensively to the incoming perturbation than the inner side.

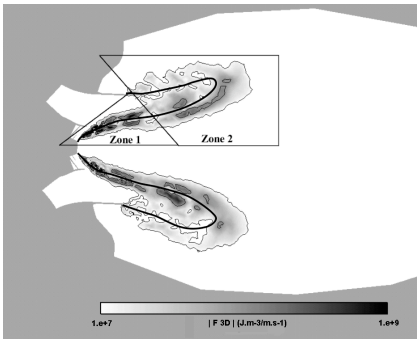

Figure 10: 2D longitudinal cut colored with the amplitude of FTF: **HF-FFT method**. Black line marks the mean flame position.

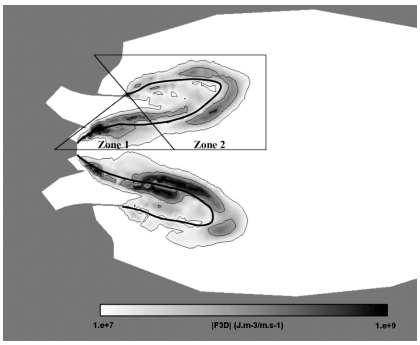

Figure 11: 2D longitudinal cut colored with the amplitude of FTF: **WN-WH method**. Black line marks the mean flame position.

7.2.2 Time delay

Figures 12 and 13 show 2D longitudinal plane cuts colored by the time delay of the FTF at 90Hz respectively obtained using the HF-FFT and WN-WH

methods. The delays change between 0 and 11 ms (the forcing period at 90Hz). The zones described for the amplitude analysis are also present on those figures. They also correspond to different types of responses:

- In zone 2, the behaviour of the time delay for the present flame is well described by the 1D analysis, with lower time delays after the mean flame front and higher time delays in the inner fluctuating area.
- In zone 1, the distribution of time delays is reversed: shorter time delays are observed before the mean flame front. It is due to the fact that the flame first contracts in the cycle, burning nearer to the injection, and then expands to reach the black zone which corresponds to higher time delays.

The dimensions of the two zones are different whether the flame is forced with a harmonic signal or with filtered white noise. It shows that even if the global time delay is almost the same for the two forcing methods, the influence of the other frequencies present with WN-WH method changes the local response of the flame (i.e. the localisation of zones 1 and 2) at 90Hz.
The maps of amplitudes (Fig.(10) and (11)) and of local time delays (Fig.(12) and (13)) exhibit obvious structures. Their interpretation however is difficult. Zone 1 seems to be the place where the most intense interaction takes place, while zone 2 yields more diffuse flame responses but with time delays which exhibit the pattern of oscillating 1D flames. This suggests that the inner flame, stabilized on the axial swirler hub, is the most unstable one and the first source of the flame response.

7.2.3 Weighted Probability density functions of time delays.

The 3D fields of amplitude and time delay obtained with both methods are used to reconstruct the Weighted-PDF of time delays. These Weighted PDF of time delays are defined by:

$$P_\omega(\tau_0 \leq \tau_\omega \leq \tau_0 + d\tau_0) = \frac{\sum_1^{n_{d\tau_0}} norm_i}{\sum_1^N norm_i}$$

in the region defined by:

$$|F|_{3D}(\omega, x, y, z) > \frac{|F|_{3D}(\omega, x, y, z)_{max}}{100}$$

$n_{d\tau_0}$ is the number of mesh points for which $\tau_0 \leq \tau_\omega \leq \tau_0 + d\tau_0$, N is the total number of mesh points in the volume and

$$norm_i = Int\left(\frac{100 * |F|_{3D}(x_i, y_i, z_i)}{|F|_{3D,max}}\right)$$

Figure 14 compares the two PDF of time delays. Both show a maximum around 2 ms which is the global value of the time delay at 90Hz. They also both show a peak around 6ms. It means that even if the global value of the time delay is

2ms a non negligible part of the fluctuations of heat release that occur out of phase with the inlet velocity. Figure 12 shows that this value corresponds to heat release fluctuations occurring inside the mean flame position in zone 1 and 2. The main difference between the two pdf of time delays is the probability of finding a time delay around 1 ms which is much smaller when the flame is forced with filtered white-noise. This may be due to the influence of higher frequencies on the 90Hz turbulent FTF using WN-WH method.

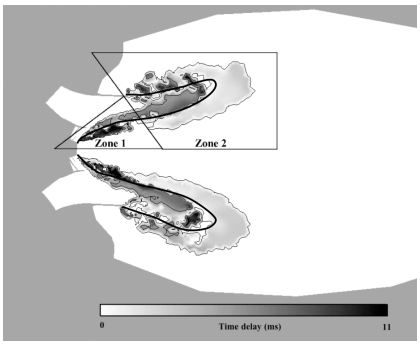

Figure 12: 2D longitudinal cut colored with the time delay of FTF: **HF-FFT method**. Black line marks the mean flame position.

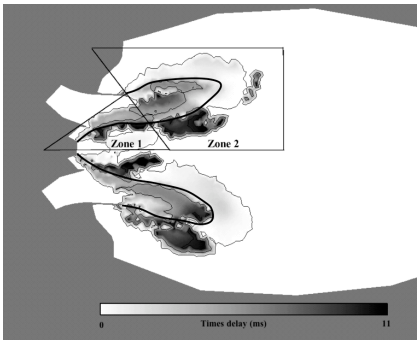

Figure 13: 2D longitudinal cut colored with the time delay of FTF: **WN-WH method**. Black line marks the mean flame position.

8 Concluding remarks

The influence of frequency on the FTF of a turbulent combustor has been studied using two different methods of forcing and post-processing. The first output of

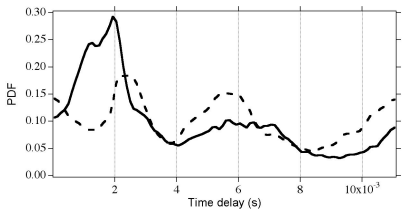

Figure 14: PDF of weighted time delays : —— WN-WH method. ▬ ▬ HF-FFT method.

this study concerns the global FTF comparison. The WN-WH method gives results that are similar to the results obtained using the harmonic method though its computational cost is much lower (4 times in this case). Yet, it has to be noticed that the white-noise forcing method requires the use of the Wiener-Hopf relation inversion and therefore has specific drawbacks that have to be carefully addressed.

- First the WH method is very sensitive to the size of the filter used for the inversion. The number of elements of the filter multiplied by the time sampling of the signal represents the time memory of the system. When inverted, this time represents the minimum frequency this method will be able to treat. But due to the matrix inversion, the size of the filter also has to remain as low as possible to give precise results. This leads to an optimal value of the size of the filter which may be sometimes hard to find.

- When forcing with white noise, extreme care has to be given to the filter cut-off frequency and to the type of filter used. In this study, the cut-off frequency is set to 600Hz which has been shown as too close to the frequencies of interest. A fourth-order low-pass filter has also been used to avoid any unwanted high frequency influences on the measured FTF.

The local response of the turbulent flame is studied at 90Hz. Both methods (HF-FFT and WN-WH) give similar FTF and probability density functions of time delays. They both show that the local response of the turbulent flame can be very different from its global response, with locations where the fluctuations of HR can be out of phase with the fluctuations of velocity even though the global response is almost in phase.

An important aspect of this study is their link with stability analysis of combustors. Obviously, FTF do have an influence on the frequency and amplification rates of modes in the numerical methods used for combustor stability [41, 42]. The present results show that methods like WN-WH and HF-FFT provide slightly different local FTF maps. Whether these differences will affect or not significantly the frequencies and amplification rates of modes remains to be studied. What this study has shown is how to construct FTFs which is the

important "brick" of acoustic analysis. Note also that experimental results on global FTF are available but that no-one has studied local FTF yet. This is obviously a required step for the future.

References

[1] A. Giauque, L. Selle, T. Poinsot, H. Buechner, P. Kaufmann, and W. Krebs. System identification of a large-scale swirled partially premixed combustor using les and measurements. *J. of Turb.*, 6(21):1–20, 2005.

[2] X. Wu, M. Wang, and P. Moin. Combustion instability due to the nonlinear interaction between sound and flame. *Center for turbulence Research Annual Research Briefs. Stanford University*, pages 131–142, 2001.

[3] W. Polifke and T. Sattelmayer. Assessment of methods for the computation of the linear stability of combustors. *Combustion Science and Technology*, 175:453–476, 2003.

[4] L. Selle, G. Lartigue, T. Poinsot, R. Koch, K.-U. Schildmacher, W. Krebs, B. Prade, P. Kaufmann, and D. Veynante. Compressible large-eddy simulation of turbulent combustion in complex geometry on unstructured meshes. *Combust. Flame* , 137(4):489–505, 2004.

[5] T. Schuller, D. Durox, and S. Candel. Self-induced combustion oscillations of laminar premixed flames stabilized on annular burners. *Combust. Flame* , 135:525–537, 2003.

[6] W. Krebs, P. Flohr, B. Prade, and S. Hoffmann. Thermoacoustic stability chart for high intense gas turbine combustion systems. *Combust. Sci. Tech.* , 174:99–128, 2002.

[7] F. Nicoud and T. Poinsot. Thermoacoustic instabilities: should the rayleigh criterion be extended to include entropy changes ? *Combust. Flame* , 142:153–159, 2005.

[8] K. Truffin and T. Poinsot. Comparison and extension of methods for acoustic identification of burners. *Combust. Flame* , 142(4):388–400, 2005.

[9] F.E.C Culick. Some recent results for nonlinear acoustic in combustion chambers. *AIAA Journal* , 32(1):146–169, 1994.

[10] Y. Huang and V. Yang. Bifurcation of flame structure in a lean-premixed swirl-stabilized combustor : transition from stable to unstable flame. *Combustion and Flame*, 136:383–389, 2004.

[11] L Crocco. Aspects of combustion instability in liquid propellant rocket motors. part i. *J. American Rocket Society* , 21:163–178, 1951.

[12] B. Schuermans, W. Polifke, and C.O. Paschereit. Modeling transfer matrices of premixed flames and comparison with experimental results. In *Int'I Gas Turbine & Aeroengine Congress & Exposition*, Indianapolis/Indiana, 1999. ASME paper.

[13] W. Polifke, A. Poncet, C.O. Paschereit, and K. Doebbeling. Reconstruction of acoustic transfer matrices by instationnary computational fluid dynamics. *J. Sound Vib.* , 245(3):483–510, 2001.

[14] W. Polifke and A. Gentemann. Order and realizability of impulse response filters for accurate identificationn of acoustic multi-ports from transient cfd. In *Tenth international congress on sound and vibration*, 2003.

[15] S.W. Yuen, A. Gentemann, and W. Polifke. Influence of boundary reflection coefficient on the system identifiability of acoustic two-ports. In *Eleventh International congress on sound and vibration*, 2004.

[16] B. Schuermans, H. Luebcke, D. Bajusz, and P. Flohr. Thermoacoustic analysis of gas turbine combustion systems using unsteady cfd. In *Proceedings of ASME Turbo Expo GT2005-68393*, 2005.

[17] C. Angelberger, F. Egolfopoulos, and D. Veynante. Large eddy simulations of chemical and acoustic effects on combustion instabilities. *Flow Turb. and Combustion* , 65(2):205–22, 2000.

[18] D. Caraeni, C. Bergstrom, and L. Fuchs. Modeling of liquid fuel injection, evaporation and mixing in a gas turbine burner using large eddy simulation. *Flow Turb. and Combustion* , 65:223–244, 2000.

[19] O. Colin and M. Rudgyard. Development of high-order taylor-galerkin schemes for unsteady calculations. *J. Comput. Phys.* , 162(2):338–371, 2000.

[20] H. Pitsch and L. Duchamp de la Geneste. Large eddy simulation of premixed turbulent combustion using a level-set approach. *Proc of the Comb. Institute*, 29:2001–2005, 2002.

[21] V. Sankaran and S. Menon. Les of spray combustion in swirling flows. *J. of Turb.*, 3:011, 2002.

[22] C. Prière, L.Y.M. Gicquel, A. Kaufmann, W. Krebs, and T. Poinsot. Les of mixing enhancement : Les predictions of mixing enhancement for jets in cross-flows. *J. of Turb.*, 5:1–30, 2004.

[23] F. Nicoud and F. Ducros. Subgrid-scale stress modelling based on the square of the velocity gradient. *Flow Turb. and Combustion* , 62(3):183–200, 1999.

[24] O. Colin, F. Ducros, D. Veynante, and T. Poinsot. A thickened flame model for large eddy simulations of turbulent premixed combustion. *Phys. Fluids* , 12(7):1843–1863, 2000.

[25] S. Roux, G. Lartigue, T. Poinsot, U. Meier, and C. Bérat. Studies of mean and unsteady flow in a swirled combustor using experiments, acoustic analysis and large eddy simulations. *Combust. Flame* , 141:40–54, 2005.

[26] L. Selle, G. Lartigue, T. Poinsot, P. Kaufman, W. Krebs, and D. Veynante. Large eddy simulation of turbulent combustion for gas turbines with reduced chemistry. In *Proceedings of the Summer Program*, pages 333–344. Center for Turbulence Research, 2002.

[27] L. Crocco. Research on combustion instability in liquid propellant rockets. In *12th Symp. (Int.) on Combustion*, pages 85–99. The Combustion Institute, Pittsburgh, 1969.

[28] G. Hsiao, R. Pandalai, H. Hura, and H. Mongia. Combustion dynamic modelling for gas turbine engines. In *98-3380, AIAA Paper*, 1998.

[29] U. Krueger, J. Hueren, S. Hoffmann, W. Krebs, P. Flohr, and D. Bohn. Prediction and measurement of thermoacoustic improvements in gas turbines with annular combustion systems. In ASME Paper, editor, *ASME TURBO EXPO*, Munich, Germany, 2000.

[30] C.O. Paschereit, P. Flohr, and B. Schuermans. Prediction of combustion oscillations in gas turbine combustors. In AIAA Paper 2001-0484, editor, *39th AIAA Aerospace Sciences Meeting and Exhibit*, Reno, NV, 2001.

[31] T. Poinsot and D. Veynante. *Theoretical and numerical combustion*. R.T. Edwards, 2001.

[32] S. Ducruix and S. Candel. External flow modulation in computational fluid dynamics. *AIAA Journal* , 42(8):1550–1558, 2004.

[33] T. Poinsot and S.K. Lele. Boundary conditions for direct simulation of compressible viscous flows. *J. Comput. Phys.* , 101:104–129, 1992.

[34] M. Giles. Non-reflecting boundary conditions for euler equation calculations. *AIAA Journal*, 28(12):2050–2058, 1990.

[35] A. Kaufmann, F. Nicoud, and T. Poinsot. Flow forcing techniques for numerical simulation of combustion instabilities. *Combust. Flame* , 131:371–385, 2002.

[36] V. Moureau, G. Lartigue, Y. Sommerer, C. Angelberger, O. Colin, and T. Poinsot. High-order methods for dns and les of compressible multicomponent reacting flows on fixed and moving grids. *J. Comput. Phys.* , 202(2):710–736, 2005.

[37] A. Sengissen, A. Giauque, G. Staffelbach, M. Porta, W. Krebs, P. Kaufmann, and T. Poinsot. Large eddy simulation of piloting effects on turbulent swirling flames. *In press in Proc. of the Combustion Institute*, 31, 2006.

[38] G. Staffelbach, L.M.Y. Gicquel, and T. Poinsot. Highly parallel large eddy simulations of multiburner configurations in industrial gas turbines. In *The Cyprus International Symposium on Complex Effects in Large Eddy Simulation*, 2005.

[39] P. Schmitt. *Simulation aux grandes échelles de la combustion étagée dans les turbines à gaz et son interaction stabilité-polluants-thermique.* PhD thesis, INP Toulouse, 2005.

[40] N. Syred. A review of oscillation mechanisms and the role of the precessing vortex core (pvc) in swirl combustion systems. *Progress in energy and combustion science (Prog. energy combust. sci.)*, 32(2):93–161, 2006.

[41] L. Benoit and F. Nicoud. Numerical assessment of thermo-acoustic instabilities in gas turbines. *International Journal for Numerical Methods in Fluids*, 47:849–855, 2005.

[42] F. Nicoud, L. Benoit, C. Sensiau, and T. Poinsot. Acoustic modes in combustors with complex impedances and multidimensional active flames. *AIAA Journal*, in press, 2007.

9 Appendix

9.1 Normalization of the global FTF

The global FTF can be normalized to enable to compare results from one configuration to an other. In this case, the transfer function F is defined by:

$$\frac{\gamma-1}{\gamma p_0 S_{inj}} \int_V \dot{\omega}'_T(t)dv = F(\omega)u'(t) \tag{9}$$

where S_{inj} is the forced reference inlet surface, $\dot{\omega}'_T$ and u' are respectively the local heat release and the inlet velocity fluctuations taken at the reference point. This normalization is introduced by analytical calculation of the asymptotic behavior for infinitely low frequency flame response as derived in [35] and presented below : for premixed flames, this asymptotic value links the ratio of burnt gas temperature (T_b) and fresh gas temperature (T_f) with the amplitude of the flame response to infinitively low frequency forcing.
Replacing integral heat release by fuel consumption in Eq.(9) and balancing fuel consumption with fuel supply leads to :

$$QS_{inj}u_{inj}\rho_0 Y_F = \int_V \dot{\omega}_T dv \tag{10}$$

where Q is the heat released by the combustion of $1kg$ of fuel. Then in the low frequency limit ($\omega \to 0$), an estimate can be derived for the limit value of the amplitude of the FTF ($|F(\omega)|$) :

$$|F(\omega)|(\omega \to 0) = \frac{\gamma-1}{\gamma p_0} Q\rho_0 Y_F^0 min(1, 1/\phi) \tag{11}$$

Assuming constant heat capacity ($c_p(T_b - T_f) = QY_F^0 min(1, 1/\phi)$), the previous equation can be written:

$$\lim_{\omega \to 0} |F(\omega)| = \frac{T_b}{T_f} - 1 \tag{12}$$

which can be a useful upper limit for $F(\omega)$. For typical methane flames, it lies between 1 and 10, depending on the inlet temperature.